Korean Journal of Remote Sensing, Vol.20, No.5, 2004, pp.337~351

Development of PKNU3: A small-format, multi-spectral, aerial photographic system

Eun-Khung Lee, Chul-Uong Choi, and Yong-Cheol Suh

Department of Satellite Information Sciences, Pukyong National University, Korea

Abstract : Our laboratory originally developed the compact, multi-spectral, automatic aerial photographic system PKNU3 to allow greater flexibility in geological and environmental data collection. We are currently developing the PKNU 3 system, which consists of a color-infrared spectral camera capable of simultaneous photography in the visible and near-infrared bands; a thermal infrared camera; two computers, each with an 80-gigabyte memory capacity for storing images; an MPEG board that can compress and transfer data to the computers in real-time; and the capability of using a helicopter platform. Before actual aerial photographic testing of the PKNU3, we experimented with each sensor. We analyzed the lens distortion, the sensitivity of the CCD in each band, and the thermal response of the thermal infrared sensor before the aerial photographing. As of September 2004, the PKNU3 development schedule has reached the second phase of testing. As the result of two aerial photographic tests, R, G, B and IR images were taken simultaneously; and images with an overlap rate of 70% using the automatic 1-s interval data recording time could be obtained by PKNU3. Further study is warranted to enhance the system with the addition of gyroscopic and IMU units.

We evaluated the PKNU 3 system as a method of environmental remote sensing by comparing each chlorophyll image derived from PKNU 3 photographs. This appraisement was backed up with existing study that resulted in a modest improvement in the linear fit between the measures of chlorophyll and the RVI, NDVI and SAVI images stem from photographs taken by Duncantech MS 3100 which has same spectral configuration with MS 4000 used in PKNU3 system.

Key Words : Multi-spectral Automatic Aerial Photographic system, PKNU 3, Thermal Infrared Sensor, Multi-spectral Camera.

1. Introduction

The development of the small-format, aerial photographic system designated PKNU2 began in June 2001 in the PE & RS Lab (Remote Sensing Center) at Pukyong National University, South Korea, and has progressed through the sixth testing phase as of June 2003. The PKNU2 system was created to obtain low-cost, useful data that are highly accurate in the spatial resolution of a target area and can be collected in a timely manner. An orthophoto map (planimetric accuracy: 0.78m, vertical accuracy: 0.83m) was produced as a test of the basic ability of PKNU2 to integrate with a GPS survey, as well as to verify and

Received 19 September 2004; Accepted 4 October 2004.

calibrate the camera lens. However, a shortcoming prevented perfect R, G, B, and IR composite images: because the RGB and infrared images were taken with separate cameras, the color-infrared composite images had to be produced in the post-processing stage, even though the vertical photos with a spatial-resolution as high as 0.29 m could be obtained using PKNU2. Thus, the objective in designing PKNU3 was to develop a platform with an enhanced, multi-spectral, aerial photographic capability, while PKNU2 would be developed further into a high spatial-resolution photographic platform.

There is considerable demand in Korea for general aerial photography and general panoramic photography, so there is a wide scope for developing and increasing the availability of these techniques. However, large-scale aerial photography dominates the photographic field owing to several problems. Therefore, relatively little aerial photography is available for scientific interpretation. Elsewhere in the world, multi-spectral photography for the detection of environmental changes and for scientific investigation is becoming a lucrative business. In particular, several studies have used aerial photographs for deadwood inventories and snag quantification, including mapping of deadwood in insect outbreak areas (Nüsslein *et al.*, 1997) and windfall areas (Scherrer, 1993; Schmidtke, 1993; Koch *et al.*, 1998). In marine studies, remote sensing using cameras and sensors mounted on aircraft have been used to quantify benthic chlorophyll by measuring the amount of reflected sunlight in the visible and near-infrared parts of the electromagnetic spectrum (Riethmuller *et al.*, 1998; Hakvoort *et al.*, 1998; Hagerthey *et al.*, 2002). Intertidal mudflats are difficult environments to sample because they are accessible only during low tides, thus limiting the time and area over which the samples can be acquired. Benthic micro-algae are normally sampled indirectly by measuring the concentration of chlorophyll at the surface, which is a time-consuming and expensive process that destroys the sampling area, making it impossible to observe the same area at frequent intervals. This latter point is an important limitation for studies that seek to quantify the temporal variation of micro-algae at the same location, e.g., over a single tidal cycle (Underwood and Kromkamp, 1999). Trampling and disturbance of study sites may also alter the characteristics of the sediment and its micro-algal assemblages, which may in turn impact the experiment. Sampling of random point-locations cannot provide the contiguous small-scale measurements necessary to provide a complete picture of chlorophyll variability over an area of mudflat (Murphy *et al.*, 2004). Airborne infrared images show the ground temperature distribution and can be acquired under almost all weather conditions. Therefore, infrared images can be widely used to investigate the water content of soil and crops, the water temperature of ocean, geology, and land classification of cities (Shukai, 1992).

With this background in mind, we developed PKNU3, a small-format, multi-spectral, aerial photographic system. PKNU3 is composed of two parts: a data storage system and a sensor portion, consisting of a thermal IR camera and a spectral camera, which is capable of taking images of R, G, B, and IR bands simultaneously. A mobile-mapping multi-spectral system like the PKNU series (2, 3) is thus the product of integrating the concepts of kinematic geodesy and digital photogrammetry. This system can be used to acquire, store, and process measurable quantities that sufficiently describe spatial and/or physical characteristics of part of the Earth's surface.

The multi-spectral sensor (MS 4000) that is loaded with the multi-spectral aerial photographic system (PKNU3) uses a triple CCD (R, B, and G; and IR), which differs from the single CCD used by general cameras; this permits acquisition of images with greater sensitivity in each band. We estimated the characteristics of the camera's lens distortion, the sensitivity in each

band of each CCD, and the sensitivity of the thermal infrared sensor for acquiring more accurate images before actual flights. Few studies in current literatures discuss the correction of lens distortion in digital cameras. Jeong and Kim (2002) performed a related study that developed a program to correct the lens distortion of CCD cameras for mobile mapping systems. Mason *et al.* (1997) and Fraser *et al.* (1997) discussed lens distortion in their studies on the possibility of generating a digital map of a small area using the Kodak DCS460 camera. In a study using color infrared (CIR) aerial photos based on ground-truth data to measure the amount of chlorophyll on an exposed mudflat (Murphy *et al.*, 2004), an 18% reflective Kodak grey card was used as a reflectance standard to calibrate the camera data for variations in incoming solar radiation.

2. Materials and Methods

1) Chronological table of this study

This study was initiated in January 2004. The field study, supported by the Ministry of Maritime Affairs and Fisheries and the Korea Environmental Institute, was completed with the second aerial photographic test

Table 1. Chronology of this study.

Date	Contents	Purpose
1/2004	Investigation of native and foreign references	Collect materials for development of the system
3/2004	Introduction of Redlake MS 4000 multi-spectral sensor	Purchase equipment for the study
3-7/2004	Development of the data storage system	Store still and moving pictures
5/2004	Evaluation of the possibility of using PKNU3 onboard helicopters	System development and safety
5-9/2004	Manufacture of gimbals for sensors	Prevention of vibration onboard helicopter
6-9/2004	Connecting cable between sensors and data storage system	The pursuit of safety and convenience
7-8/2004	Geometric and radiometric corrections of sensors	Evaluation of sensor characteristics
9/9/2004	First aerial photographic test	Estimation of system's fundamental capacity
9/14/2004	Second aerial photographic test	Possibility of high-volume photography with multi-spectral data

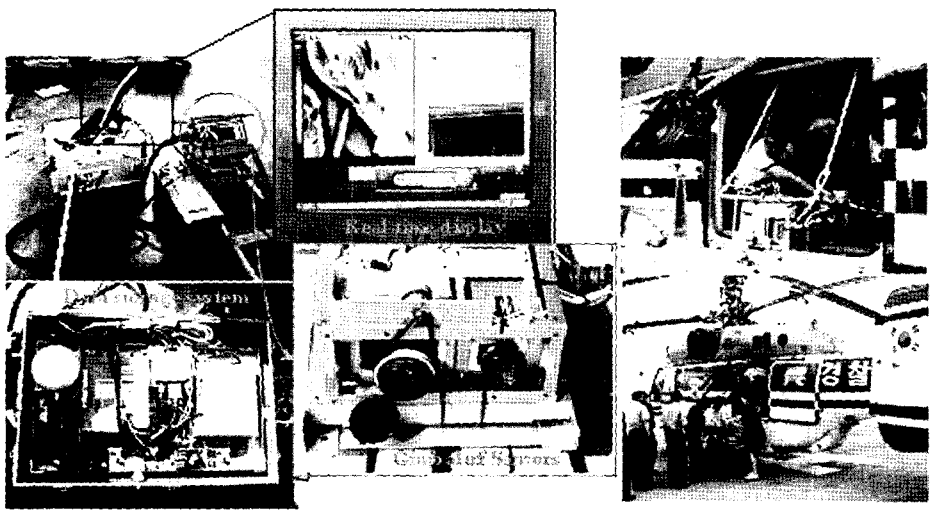

Fig. 1. Multi-spectral aerial photographic system and platform.

in September 2004. The objectives of each test are shown in Table 1.

2) PKNU3 multi-spectral aerial photographic system

The PKNU3 system consists of a sensor array, a data storage system, and a platform (Fig. 1). The sensor portion uses a Redlake MS 4000 (Redlake, San Diego, CA) multi-spectral camera and a Raytheon IRPro thermal IR camera, which are both supported by gimbals to compensate for vibrations of the platform and to allow for adjustments of the photographic angle. The data storage system is composed of an MPEG board, which can compress and transfer moving pictures as high quality images in real time, and two computers, each with an 80-gigabyte memory capacity for data storage. Helicopters were chosen as the aerial platform over fixed-wing aircraft because they can rotate 360° and fly at low speeds.

(1) Sensor portion

The PKNU2 system had drawbacks in its ability to obtain composite, four-band images of any particular target area because the tasks of photographing the color and near-infrared images were divided between the separate Kodak DCS 460 color and infrared cameras, respectively. In addition, it was difficult to control the minimum overlap rate (60%) owing to the 12-s storage delay. The Redlake MS 4000 sensor was introduced to overcome these drawbacks as well as to provide the capability of obtaining moving picture data.

The Redlake MS 4000 sensor is a triple-CCD camera that can simultaneously take images in the R, G, B, and IR bands, thus producing RGB and CIR images of the target area at 1600 × 1200 pixels (7.4 μm per pixel). The light sensitivity of the camera lens is controlled by using gain values and an electronic shutter. The camera was fitted with a Nikkon F-mount, 20-mm F2.8 rectillinear lens. The Raytheon IRPro thermal infrared camera used in this study senses the energy of the 7~14 μm wavelength as still and moving pictures and displays them through an LCD viewer. The distribution of the thermal energy in images can be displayed through the use of five colors (red, orange, yellow, green, and blue), and temperatures can be shown in terms of brightness values. This camera was fitted with a Raytheon 50-mm F-1 lens. These two cameras (Redlake MS 4000 and Raytheon IRPro) were mounted on the gimbals that were specially designed to prevent platform vibration and to allow a wide range of adjustments of the photographic angle. While the MS 4000 has autofocus, the thermal IR camera does not; therefore, a separate unit was added to the gimbals/camera assembly to focus the thermal IR camera remotely.

(2) Data storage system

A high-capacity data storage system is necessary to record the volumes of images because of the 1-s data storage time of the MS 4000. Two compact computers were implemented for the data storage system, each with a storage capacity of 80 gigabytes and a 12-volt power supply. The two computers were tightly packaged in a special case that insulated them from the vibration of a helicopter platform. To further reduce vibration, a wiring harness was used that consolidated every connector between the sensor components and the data storage system into one thick cable.

(3) GPS

A technique to acquire the exterior orientation parameters directly through combining several sensors in aerial reconnaissance aircraft was recently developed by Ackermann (1993). GPS photogrammetry and GPS/INS photogrammetry allows the acquisition of exterior orientation parameters with only the use of a minimum of ground control points. The ground control process could even be completely skipped with a 30~50% reduction of the total cartography cost (Park *et*

al., 2004). Various applications in GIS, airborne remote sensing, and resource mapping often require data capture in fully digital form, with sufficient accuracy, speed, and cost-effectiveness. Therefore, integrated digital image acquisition and navigation systems have been developed for such applications (Cramer *et al.*, 1997; Mostafa *et al.*, 1997; Toth and Grejner-Brzezinska, 1998).

In this research, a GPS antenna was included in PKNU3 to compute the flight course, flight velocity, and altitude of an aerial platform, as well as to provide the three-dimensional coordinates (x, y, z) of each exposure location and a kappa value(K) among the rotation angles (ω, ϕ, K) of the platform for exterior orientation.

3) Calibration and correction of sensors

Prior to obtaining data from aerial photography, the sensor was calibrated to ensure that geometric and radiometric distortions of PKNU3 system itself are excluded.

(1) Geometric correction of a multi-spectral camera (RGB/CIR MS 4000 sensor)

Camera lens distortion resulting from the geometric structure of a lens is divided into radial distortion and tangential distortion. Tangential distortion is generally of much less consequence than radial distortion and can often be disregarded entirely; therefore, in this investigation, we performed calibration and correction only for radial distortion according to the following method.

A panel composed of 121 GCPs at regular intervals was surveyed using a theodolite for correcting the radial lens distortion, and an image of the panel was taken with the MS 4000 sensor. The ground coordinates (x, y, z) were calculated using the horizontal angle (HA), vertical angle (VA), and slope distance (SA) as surveyed by theodolite; the radial distance of ground coordinates, the radial distance of an image (r), and the radial distortion (Δr) were computed.

Table 2. Precision.

Image precision	X (pixel)	Y (pixel)	RMSE
Before correction for lens distortion	0.9374	0.8530	0.9195
After correction for lens distortion	0.6789	0.4936	0.5736

The lens distortions were computed by comparing the ground coordinates (reference) surveyed by theodolite with the converted coordinates from the pixel numbers on the image of the panel in this paper. The lens distortion was evaluated by using Eq. (1) with the following coefficients: $K_0 = 6.4817200e^{-3}$, $K_1 = -4.4270500e\text{-}4$ and $K_2 = 3.9596100e^{-6}$.

$$\Delta r = k_0 r + k_1 r^3 + k_2 r^5 + \cdots + k_n r^{2n-1} \quad (1)$$

where Δr is the radial distortion, r: is the radial distance, k0 through kn are the coefficients of radial distortion, and υ is the variation.

The image coordinate (x, y) corrections for the radial lens distortion were calculated from Eq. (2). The precision of x and y and the root mean square error (RMSE) of the image before and after the correction for the lens distortion are shown in Table 2.

$$x = x - \frac{x}{\gamma}\Delta\gamma,\ y = y - \frac{y}{\gamma}\Delta\gamma \quad (2)$$

To obtain as little as 0.57~0.92 pixel lens distortion, we used only the central part of a CCD, which represents 12% of the available photographic area, as this area has the least lens distortion. It was possible to obtain images geometrically with a lens distortion of less than 1 pixel in size through calibration of the Redlake MS 4000 sensor for lens distortion.

(2) Radiometric correction of the multi-spectral camera (RGB/CIR MS 4000 sensor)

The measurements made by the multi-spectral sensor must be calibrated with the spectrometer measurements of the energy emitted and reflected by an object. Radiometric corrections should be conducted to obtain the actual intensity of solar radiant energy and reflectance. The ability of the MS 4000 to photograph multi-spectrally

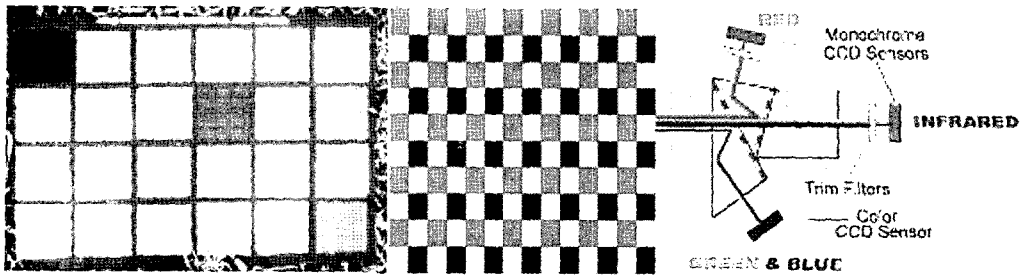

Fig. 2. Macbeth Color Checker & Bayer mosaic patterns of pixel filters & MS 4000 RGB/CIR configuration (from left).

was evaluated by verification of the radiometric distortion. To compare and analyze between the ground-truthing data and pixel values on the image, the Macbeth Color Checker (GretagMacbeth Corp., New Windsor, NY; Fig. 2) was used; the results are shown in Table 3.

The correlations between the brightness values on the image and the measured solar radiant energy were analyzed at different f-stops (2.8, 8, 11, 16) and exposure times to determine the maximum and minimum quantized calibrated pixel values (QCAL; effective sensed range of the MS 4000 sensor). The effective QCALs were then converted to spectral radiance at the sensor's aperture by following Eq. (3), to compare them to the ground-truthed values of radiant energy.

$$L_\lambda = ((LMAX_\lambda - LMIN_\lambda)/(QCALMAX - QCALMIN)) \times (QCAL - QCALMIN) + LMIN_\lambda \quad (3)$$

where L_λ = spectral radiance at the sensor's aperture ($W/m^2 \cdot sr \cdot \mu m$), QCAL = the quantized calibrated pixel value in digital number (DN), $LMIN_\lambda$ = the spectral radiance scaled to QCALMIN, $LMAX_\lambda$ = the spectral radiance scaled to QCALMAX, QCALMIN = the minimum quantized calibrated pixel value (corresponding to $LMIN_\lambda$) in DN, QCALMAX = the maximum quantized calibrated pixel value (corresponding to $LMAX_\lambda$) in DN).

The gradients (Red: 8324.9, Green: 6921.8, Blue: 4773.1) in Fig.3 are the radiant energy to the spectral radiance. The more gradient increases, the less sensitivity of CCD decreases. Hence, the sensitivity of a CCD for the red band was inferior to that of the others. It is considered because a monochrome CCD sensor acquires the red plane at full resolution while it senses

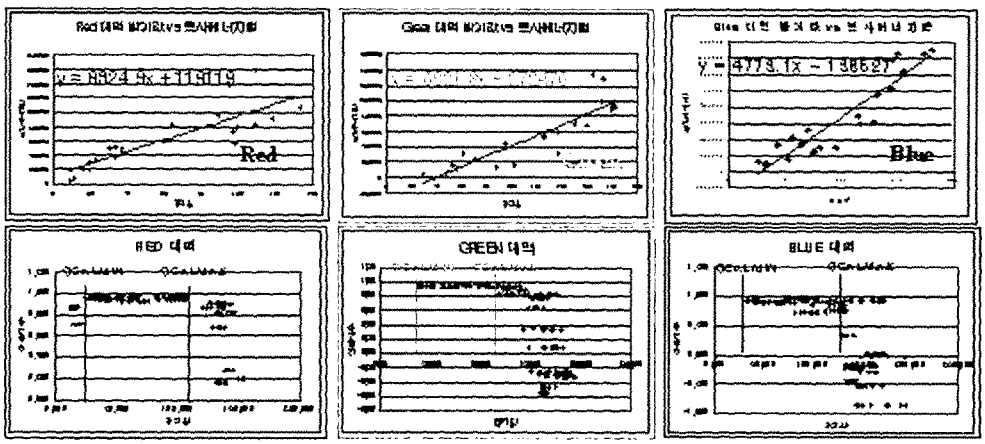

Fig. 3. Correlations between spectral radiance in effective sensed range and radiant energy & Effective sensed range of MS 4000 sensor.

Table 3. Radiometric correction in each band (RGB).

Color	Correlation factor (CF)			RGB pixel values			Ground target spectral reflectance			Spectral radiance at each band		
	B	G	R	B	G	R	B	G	R	B	G	R
Darkskin	0.67	0.50	1.70	42	61	33	11	12	22	6550.54	5910.4	11653.6
Lightskin	0.62	0.41	1.17	131	160	89	32	26	41	18476.6	13292.9	21233.9
Bluesky	0.64	0.41	1.79	144	125	30	36	20	21	20463.2	10117.7	11053.4
Foliage	1.37	0.97	3.49	56	95	19	30	36	26	16859.8	17356.4	13308.1
Blueflower	0.35	0.20	0.56	154	137	59	21	11	13	12123.7	5816.27	6514.9
Bluishgreen	0.35	0.25	0.69	155	183	37	21	18	10	12289.5	8728.59	5310.26
Moderatered	0.28	0.14	0.65	74	88	98	8	5	25	4720.16	2504.16	12872.1
Purple	0.67	0.29	1.24	69	52	33	18	6	16	10473.6	2937.26	8314.75
Yellowgre	0.24	0.79	1.36	118	174	60	11	54	32	6777.2	26723.4	17053.2
Orangeyellow	0.16	0.25	0.81	81	181	95	5	18	30	2970.86	8971.79	15656.9
Blue	0.95	0.32	1.39	116	55	11	43	7	6	23167.3	3931.41	3387.36
Green	0.16	0.31	0.70	93	150	22	6	18	6	3487.69	9313.34	3067.96
Red	0.24	0.11	0.84	32	47	109	3	2	36	1918.06	1284.68	18662.5
Yellow	0.13	0.40	0.80	95	164	109	5	26	34	2922.34	12926	17714.1
Magenta	0.22	0.08	0.41	128	102	118	11	3	19	6146.13	1685.76	9997.59
Cyan	0.74	0.46	1.43	173	150	16	50	27	9	28686.5	13656.6	4594.45
White	0.85	0.71	0.68	180	173	177	60	48	47	34644.5	24648.8	24497.8
Netual8	1.41	0.94	1.63	154	180	97	85	66	62	48610.5	33959.9	32490.3
Netua6.5	0.83	0.55	1.39	145	171	64	47	37	35	27061.8	18899.5	18289.7
Netua5	1.06	0.84	2.62	115	125	37	48	41	38	27506.9	20790.7	20048.2
Netua3.5	1.00	0.68	2.28	64	71	19	25	19	17	14039.2	9760.06	9022.75
Black	0.39	0.18	0.57	26	29	9	4	2	2	2380.63	994.472	1169.23
Average	0.61	0.45	1.28									

the green (50%) and blue (25%) bands on the same CCD with a Bayer pattern as shown in Fig.2 to balance on R, G, and B sensitivity.

The calibration between the measured RGB reflectance of the color chart and the RGB values of the image (i.e., the radiometric correction) was performed by calculating the correlation factor (CF) values from Eq. (4).

$$CF = \text{Ground target spectral reflectance} / (\text{RGB values}/255) \quad (4)$$

The RGB sensitivity of the sensor was calculated using CF values (Ron Graham *et al.*, 2002). According to the CF values, the MS 4000 was more sensitive for the G/B bands than for the R band. To maintain a proper balance among the R, G, and B bands of an image, the gain value was adjusted to increase or decrease the response to the light reaching the CCD through the camera lens in the G and B bands and the R band, respectively.

(3) Evaluation of characteristics of thermal infrared sensor

If the emissivity (ε) of an object is known, the total spectral radiant flux of an actual object can be calculated by modifying the Stefan-Bolzmann's law ($M_b = \sigma T_{kin}^4$) as applied to a black body. The following Eq. (5) takes into account the temperature and emissivity of an object for an accurate comparison between the radiant flux and the values reported on the thermal IR sensor (Chae Hyo Seog *et al.*, 2002).

$$Mr = \varepsilon T_{kin}^4 \quad (5)$$

The thermal infrared sensor generally reports the outward radiant temperature (Krad) of an object as

Table 4. Surveyed temperatures, radiant temperatures, and brightness values.

T(°C)	Concrete (1)			Concrete (1)			Wall			Grass		
Time	T	RT	BV	T	RT	BV	T	RT	BV	T	RT	BV
11:50	33.2	32.3	217	36.6	35.6	153	27.4	26.7	73	30.7	29.9	124
12:05	31.8	31	222	36	25.1	162	27.3	26.6	75	28.8	28.1	119
12:20	31.1	30.3	224	35.1	34.2	193	27.1	26.4	76	27.6	26.9	115
⋮	⋮	⋮	⋮	⋮	⋮	⋮	⋮	⋮	⋮	⋮	⋮	⋮
17:35	28	29.3	134	31.3	30.5	107	165	25	24.4	48		
17:50	27.9	27.2	119	30.6	29.8	94	174	25	24.4	56		
18:05	27.4	26.7	117	29.3	28.5	97	157	23.9	23.3	49		

opposed to the temperature (Tkin). The relationship between the radiant temperature input of an object on a sensor and the temperature is $K_{rad} = \varepsilon^{1/4} T_{kin}$. Therefore, the radiant temperature was calculated for each object with regard to emissivity in order to analyze the correlation with brightness values for an image, as shown in Table 4.

The correlation coefficients between the outward radiant temperature with regard to an object's emissivity and the sensitivity of thermal IR sensor for each object were as high as 0.834 on concrete, 0.889 on a wall, and 0.725 on grass.

3. Results

1) First aerial photography test

The first test was an evaluation of the essential capabilities of PKNU3. An aerial platform (helicopter) equipped with PKNU3 left the National Maritime Police at Kimhae Airport at 24 min and 27 s past 2:00 PM and completed its flight plan at 48 min, 47 s past 3:00 PM on September 9, 2004.

According to the analysis of the recorded GPS data, the altitude of the first flight was approximately between the minimum mean sea level (MSL) of 100 m and the maximum of 450 m with a maximum flying speed of 200 km/h. We are unable to provide exterior orientation using the GPS data for this test because the GPS receiver was erroneously set to a 20-s data acquisition interval instead of the specified 1-s interval.

Pictures taken in the first test were underexposed as a result of cloudy and rainy weather and a lack of radiation intensity. Many images were out of focus as a result of miscalculation of an appropriate exposure time, because the helicopter's speed was faster than the anticipated 100 km/h. Moreover, it was difficult to

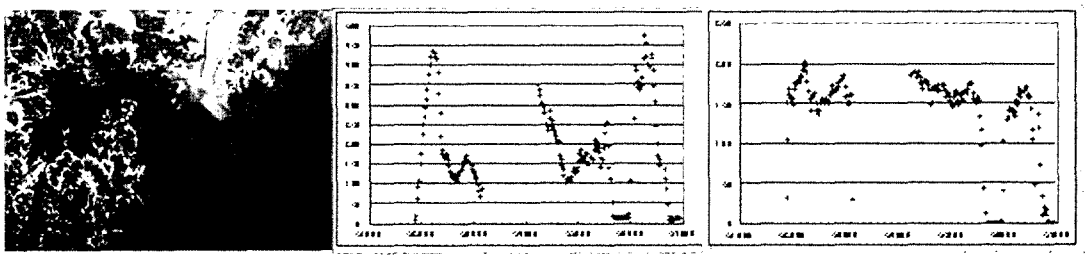

Flight course (1st: red line, 2nd: blue line) | Change of 1st flight altitude (X:Julian second, Y:Mean Sea Level(MSL)) | Change of 1st flight velocity (X:Julian second, Y:velocity(km/s))

Fig. 4. First flight course, altitude, and velocity.

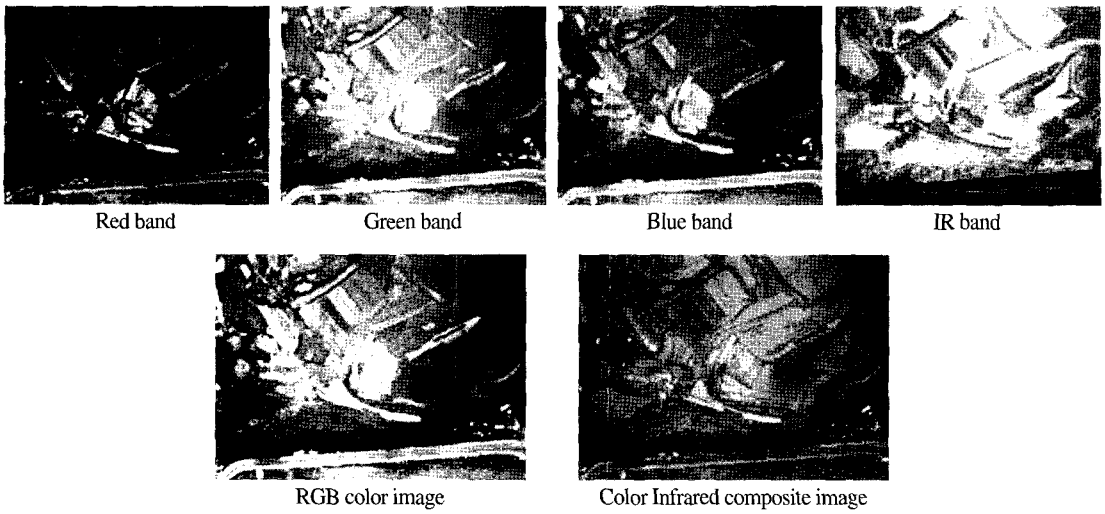

Fig. 5. Still photographs (four-band).

maintain the proper balance among the sensitivities of the R, G, B, and IR bands for each CCD sensor because a lack of radiation intensity made control of the gain value difficult.

As a result of the first test, 278 sheets (7510 Kb each = 1.96 GB) of four-band still pictures in BSQ format, 72 min of moving color pictures (722 Mb), and 2.4 GB of moving thermal infrared pictures were obtained.

2) Second aerial photography test

Second test evaluated the capability of PKNU3 to provide high-volume multi-spectral photography. The second flight began at 19 min and 40 s before 2:00 PM at Dalmaji Hill Airfield, Haeundae, Busan, and finished 25 min and 30 s past 3:00 PM at the same place, after flying over Geojedo, Tongyoung, Gaduckdo, and the port of Daebyun. According to the GPS receiver data, the flight altitude was between 100 and 400 m, and the flying speed was between 100 and 220 km/h (Fig. 6).

PKNU3 took 6200 sheets (7510 Kb each = 46.56 GB) of still pictures, 108 min of moving color pictures (4.16 GB), and 4.3 GB of moving thermal infrared pictures during the flight time of 1 h and 45 min. The photographic area per image sheet was 0.022km^2 (0.17km × 0.13km), and the spatial resolution was 0.11 m as a result of the low altitude.

The images with overlap rates of 60-70% were obtained by automatically storing data at 1-s intervals.

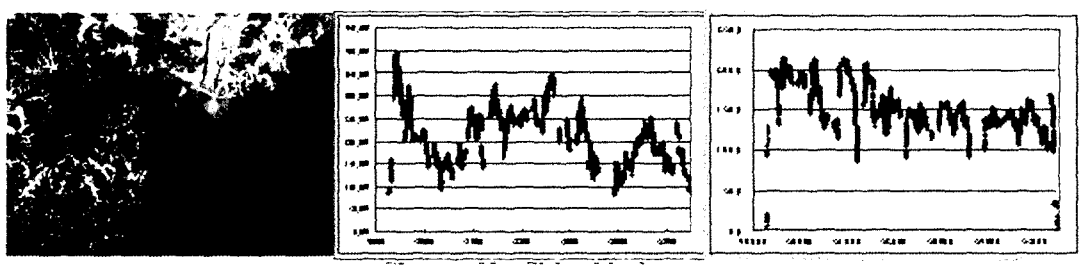

Flight course (1st: red line, 2nd: blue line)

Change of 2nd flight altitude (X:Julian second, Y:Mean Sea Level(MSL))

Change of 2nd flight velocity (X:Julian second, Y:velocity(km/s))

Fig. 6. Second flight course, altitude, and velocity.

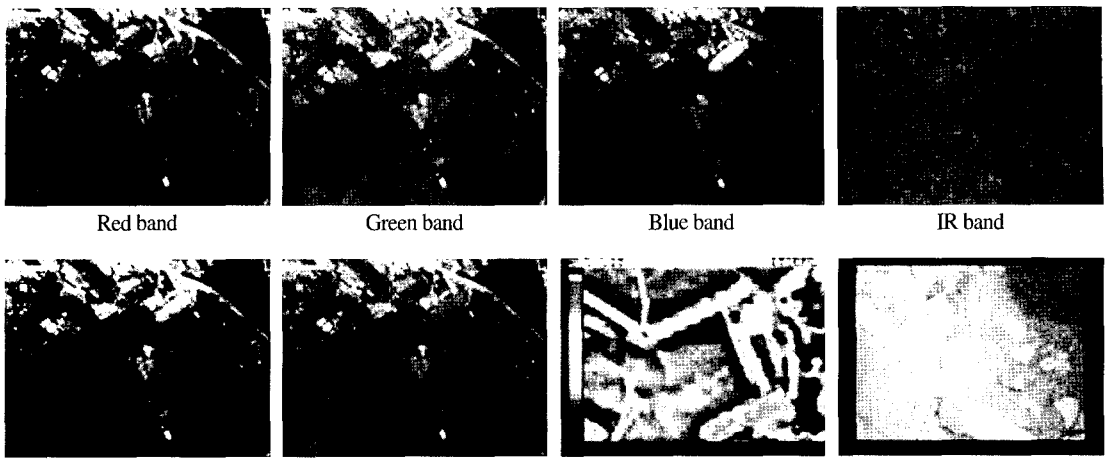

Fig. 7. Results of the second flight: Still photographs (four-band), RGB, and CIR images, and thermal IR, color moving pictures.

Table 5. Camera attributes: x, y, z, and omega (ω), phi (ϕ), kappa (κ).

time	x	y	z	Ω	ϕ	κ
14:30:31	148233	143953	269	22	17	-342
14:30:32	148223	143976	271	22	17	-338
14:30:33	148211	143999	272	22	17	-334
14:30:34	148198	144020	274	22	17	-331
14:30:35	148183	144042	275	22	17	-328
⋮	⋮	⋮	⋮	⋮	⋮	⋮
14:38:09	151429	155238	303	22	17	-65
14:38:10	151460	155257	301	22	17	-65
14:38:11	151491	155276	299	22	17	-63

The attributes of sensor shown in Table 5 include the coordinates and rotation values of the platform at each exposure station. The gain values and exposure times for each band to control the response of the CCD to the light passing through the lens were 3 in G/B bands and 6 in R and NIR bands, and 4 milliseconds for every band.

3) Application of results

Several vegetation indices were applied to imageries taken by PKNU 3 for evaluating the utility of them as a data for Environmental remote sensing. The usefulness of remotely sensed data for any application is dependent upon the acquisition of appropriate ground-truth data. However we didn't measure in situ chlorophyll to compare with the spectral indices, therefore, the practicality of PKNU3 was evaluated by an inductive method analyzing the coefficients among the spectral signatures of chlorophyll images including NDVI, RVI, SAVI, and etc., which have been already used as a way to extract the related information with covered vegetation on the earth from satellite images and aerial photographs for over 30 years. The study of Murphy *et al.*, which described a field-based method to estimate chlorophyll using digital color-infrared photograph taken by Duncantech 3-band CIR camera, having the same spectral configuration as MS4000 sensor, supports this reasoning by induction (Table 6).

The images applied each index are displayed as RGB

Table 6. Vegetation indices used in this study.

Vegetation Index	RVI(Ratio Vegetation Index)	NDVI(Normalized Difference Vegetation Index)	SAVI (Soil Adjusted Vegetation Index)	SARVI (Soil and Atmospherically Resistant Vegetation Index)
Method	$\frac{NIR}{Red}$	$\frac{NIR\text{-}Red}{NIR+Red}$	$\frac{(1+L)(NIR\text{-}Red)}{NIR+Red+L}$	$\frac{P^*_{nir} - P^*_{rb}}{P^*_{nir} + P^*_{rb} + L}$
Reference	Jordan, 1969	Rouse *et al.*, 1973	Huete,1988	Huete and Lin,1994; Running *et al.*,1994
Vegetation Index	IRGVI(Infrared/ Green ratio)	LIRGVI(Log Infrared/Green Ratio)	ARVI(Atmospherically Resistant Vegetation Index)	EVI (Enhanced Vegetation Index)
Method	$\frac{NIR}{Green}$	$\log(\frac{NIR}{Green})$	$\frac{P^*_{nir} - P^*_{rb}}{P^*_{nir} + P^*_{rb}}$ $P^*_{rb} = P^*_{red} - \gamma(P^*_{blue} - P^*_{red})$	$\frac{P^*_{nir} - P^*_{red}}{P^*_{nir} + C_1P^*_{red} - C_2P^*_{blue} + L}$
Reference	Lichtenthaler *et al.*,1996	Buschmann and Nagel, 1993	Kaufman and Tanre,1992; Huete and Lin,1994	Huete and Justice,1999

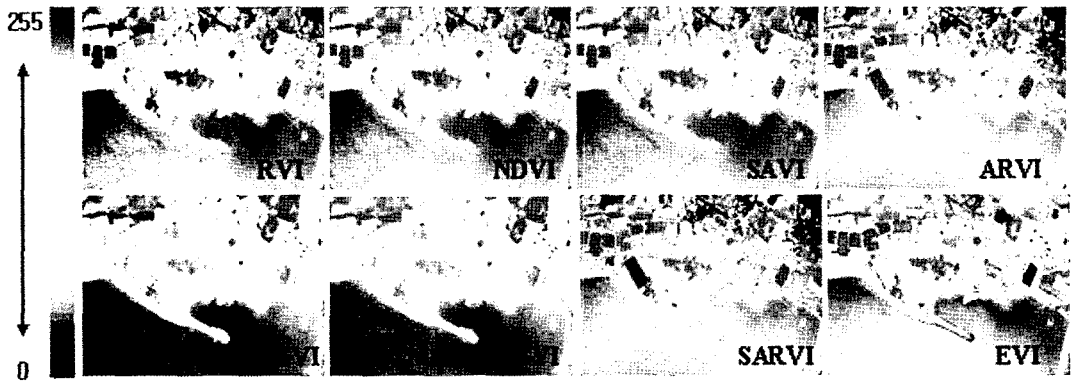

Fig. 8. Images of each vegetation index derived from PKNU 3 photos.

Table 7. Correlation coefficients among vegetation indices applied to imageries

	RVI	NDVI	SAVI	IRGVI	LIRGVI	ARVI	SARVI	EVI
RVI	1	0.99	0.99	0.70	0.65	0.82	0.82	0.47
NDVI	0.99	1	1	0.71	0.67	0.80	0.80	0.47
SAVI	0.99	1	1	0.71	0.67	0.80	0.80	0.47
IRGVI	0.70	0.71	0.71	1	1	0.22	0.22	0.71
LIRGVI	0.65	0.67	0.67	1	1	0.22	0.22	0.56
ARVI	0.82	0.80	0.80	0.22	0.22	1	1	-0.08
SARVI	0.82	0.80	0.80	0.22	0.22	1	1	-0.08
EVI	0.47	0.47	0.47	0.71	0.56	-0.08	-0.08	1

color of the range of 0-255 in Fig. 8.

The mean values of spectral signatures in imagery were calculated to analyze correlation among imageries applied vegetation indices in Table 7.

The correlation coefficients in RVI, NDVI and SAVI indices are high (Table 7) same as the result of Murphy *et al.* which resulted in a modest improvement in the linear fit between the measure of chlorophyll and the

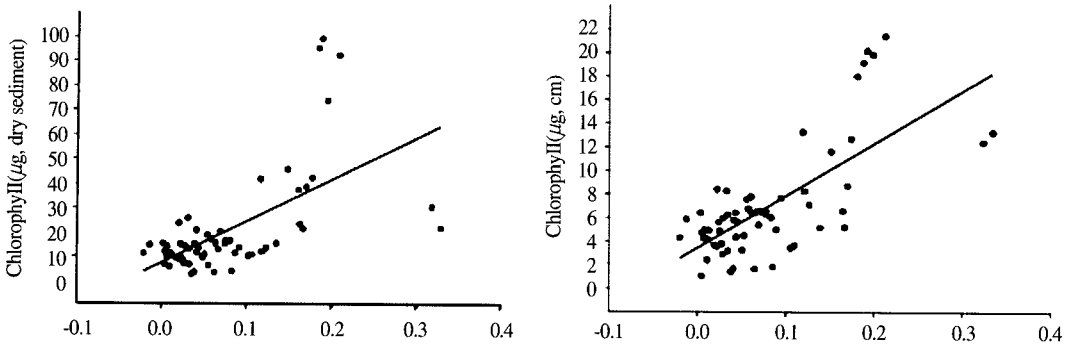

Fig. 9. Relationship between area- and weight-normalized chlorophyll and SAVI. (a) Weight-normalized chlorophyll and SAVI (R2=0.31, P<0.01, n=61). (b) Area-normalized chlorophyll and SAVI (R2=0.50, P<0.01, n=61). <The source of figure: R. J. Murphy *et al.*, 2004>

RVI, NDVI and SAVI indices(Fig.9). The distribution of chlorophyll in the RVI and NDVI images exhibits a spatial pattern almost identical to that observed in the SAVI image (Murphy *et al.*, 2004).

According to Murphy *et al.*, the field-based CIR photography will provide a useful tool for the non-destructive determination of benthic chlorophyll. Therefore, it is considered that the PKNU 3 system can be used as a method of Environmental remote sensing.

4. Conclusions

As of September 2004, the PKNU3 development schedule has reached the second phase of testing. Various experiments and tasks have been conducted to improve this system, and the following have been achieved.

First, a multi-spectral, aerial photographic system has been created that, at its core, consists of a sensor capable of taking R, G, B, and IR images simultaneously, immediately producing a composite RGB and CIR image of a target area coupled with a thermal infrared image.

Second, using the integrated data storage system, high-volume photography on long-distance flights as well as the ability to obtain images with an overlap rate of 60-70% using the automatic 1-s interval data recording time is now possible.

Third, the thermal IR sensor's lack of autofocus has been mitigated by the successful implementation of a remote focus-control system that is installed in the gimbals/camera assembly.

Fourth, to limit the lens distortion to as little as 0.57-0.92 pixels, only the central 12% of the available photographic area, where lens distortion is least, is used.

Fifth, to maintain the proper balance among the R, G, and B bands of an image, the gain values are lowered for the G/B band and raised for the R band to adjust the responses to the light reaching the CCD through the camera lens.

Sixth, the sensitivity of CCD for the red band is inferior to that for other bands because a monochrome CCD sensor acquires the red plane at full resolution whereas it senses the green and blue bands on the same CCD with a Bayer pattern.

Seventh, the correlation coefficients between the outward radiant temperature regarding an object's emissivity and the sensitivity of the thermal IR sensor for each object are as high as 0.834 for concrete, 0.889 for a wall, and 0.725 for grass.

Eighth, it was determined that the images taken during the first flight were out of focus owing to a miscalculation of the appropriate exposure time

(resulting from a lack of synchronization between the velocity of the aerial platform and the exposure calculations) and to a difficulty in maintaining a proper balance among the sensitivities of the R, G, B, and IR bands for each CCD sensor, which was attributable to inaccurate gain values as a result of the low-intensity of radiation.

Ninth, determination of appropriate exposure times and gain values during the second test were successfully accomplished, and the coordinates and rotation value (only kappa value) of the platform at each exposure station were computed from the processed GPS data. Further study is warranted to enhance the system with the addition of gyroscopic and IMU units for obtaining omega and phi values and to verify the data and calibration procedures of the system to produce strips automatically.

Tenth, the PKNU 3 data will be used as a useful tool for Environmental remote sensing. We need to measure ground-truth chlorophyll directly in the study area and compare with the other indices for proving the utility of PKNU 3 system in the future study.

Acknowledgements

We express our gratitude to the Pukyong National University, the Ministry of Maritime Affairs and Fisheries, and the Korea Environmental Institute for their support of this study.

References

Buschmann, C. and E. Nagel, 1993. In vivo spectroscopy of internal optics of leaves as basis for remote sensing of vegetation, *International Journal of Remote Sensing*, 14 (4): 711-722.

Clive S. Fraser, 1997. Digital camera self-calibration, *ISPRS Journal of Photogrammetry and Remote Sensing*, 52(4): 149-159.

Cramer, M., D. Stallmann, and N. Haala, 1997. High precision georeferencing using GPS/INS and image matching, *Proc. International Symposium on Kinematic Systems in Geodesy, Geomatics and Navigation*, Banff, Canada, pp.453- 462.

Cramer, M., D. Stallmann, and N. Haala, , 2000. Direct Georereferencing Using GPS/Inertial Exterior Orientations for Photogrammetric Applications, *ISPRS* Vol. XXXIII Part B3/1, pp.198-206.

Ackermann, F. and H. Schade, 1993. Application of GPS for Aerial Triangulation, *Photogrammetiric Engineering & Remote Sensing*, 59(11): 18-39.

Hagerthey, S. E., D. M. Paterson, and J. Kromkamp, 2002. Monitoring estuarine ecosystems: the Eden Estuary and the BIOPTIS programme. *Estuarine and Coastal Sciences Association*, 2003. Coastal Zone Topics, 5. The Estuaries and Coasts of North-East Scotland. Aberdeen, *Estuarine and Coastal Sciences Association*, pp.89-97.

Hakvoort, J. H. M., M. Heineke, K. Heyman, H. Kuhl, R. Riethmuller, and G. Witte, 1998. A basis for mapping the erodibility of tidal flats by optical remote sensing. *Marine and Freshwater Research*, 49: 867-873.

Huete, A. R., 1996. A Soil-adjusted Vegetation Index(SAVI), *Remote sensing of Environment*, 25: 295-309.

Heute, A. and C. Justice, 1999. MODIS Vegetation Index (MOD 13) Algorithm Theoretical Basis Document, Greenbelt: NASA Goddard Space Flight Center, http://modarch.gsfc.nasa.gov/MODIS/LAND/#vegetation indices, 129p.

Heute, A. F. and H. Q. Liu, 1994. An Error and Sensitivity Analysis of the Atmospheric-and Solid-Collecting Variants of the Normalized Difference Vegetation Index for the MODIS-EOS, *IEEE Transactions on Geoscience and*

Remote Sensing, 32(4): 897-905.

Huete, A. R., G. Hua, J. Qi, A. Chehbouni and W. J. Van Leeuwem, 1992. .Normalization of Multidirectional Red and Near-Infrared Reflectances with the SAVI,. *Remote Sensing of Environment*, 40: 1-20.

Jeong, D-H, and B-G. Kim, 2002. Surveying and Geo-Spatial Information Engineering: Lens Distortion Correction for CCD Camera using Projective Transformation Method, *The Korean society of Civil engineers collected papers D*, 22(5): 995-1001.

Murphy, R. J., T. J. Tolhurst, M. G. Chapman, and A. J. Underwood, 2004. Estimation of surface chlorophyll on an exposed mudflat using digital colour-infrared (CIR) photography, Estuarine, *Coastal and Shelf Science*, 59: 625-638.

Jensen J. R., H-S Chae, G-E Kim, S-J Kim, Y-S Kim, K-S Lee, K-S Cho, and M-H Jo, 2002, *Environment Remote Sensing*, Sigma Press, Prentice Hall, pp.255-297, 381-386.

Jordan, C. F., 1969. Derivation of leaf area index from quality of light on the forest floor, *Ecology*, 50: 663-666.

Koch, B., D. Münch, T. Pröbsting, 1998. Totholz als ökosystemare Eingangsgrösse, In: Fischer, A. (Ed.), *Die Entwicklung von Wald-Biozö nosen nach Sturmwurf. Landsberg, Baden-Wü rttemberg*, pp.64-73.

L. Shukai, 1992. *Analysis of Remote Sensing of Global Environment and Resources*, Surveying and Mapping Press, Beijing.

Lichtenthaler, H. K., A. Gitelson, M. Lang, 1996. Non-destructive determination of chlorophyll content of leaves of a green and an aurea mutant of tobacco by reflectance measurements, *Journal of Plant Physiology*, 148: 483-493.

Livingstone, D., J. Raper, and T. McCarthy, 1999. Integrating aerial videography and digital photography with terrain modeling, *Geomorphology*, 29: 77-92.

Mostafa, M. M. R. and K. P. Schwarz, 2001. Digital image georeferencing from a multiple camera system by GPS/INS, *ISPRS Journal of Photogrammetry & Remote Sensing*, 5(1): 1-12.

Mostafa, M. M. R., K. P. Schwarz, and P. Gong, 1997. A fully digital system for airborne mapping, *Proc. International Symposium on Kinematic Systems in Geodesy, Geomatics, and Navigation*, Banff, Alberta, Canada, pp.463-471.

Nüsslein, S., A. Greune, H. Adler, A. Troycke, G. Faisst, S. Reimeier, and R. Dietrich, 1997. *Totholzflächen und Waldstrukturdaten im Nationalpark Bayerischer Wald* (1996/1997), Bayerische Landesanstalt fur Wald und Forstwirtschaft, Dfreising.

Park, W-Y, K-W Lee, J-O Lee, and G-U Jeong, 2004, Block Adjustment with GPS/INS in Aerial Photogrammetry, *Journal of the Korean Society of Surveying, Geodesy, Photogrammetry, and Cartography*, 22(3): 285-291.

Riethmuller, R., J. H. M. Hakvoort, M. Heineke, K. Heymann, H. Kuhl, and G. Witte, 1998. Relating erosion shear stress to tidal flat surface colour. In: Black, K.S., Paterson, D.M., Cramp, A. (Eds.), Sedimentary Processes in the Intertidal Zone. Special Publications 139. *Geological Society*, London, pp.283-293.

Graham R. and A. Koh, 2002. *Digital Aerial Survey Theory and Practice*, Whittles Publishing, pp.52-121.

Rouse, J. W., R. H. Haas, J. A. Schell, and D. W. Deering, 1973. Monitoring vegetation systems in the great plains with ERTS, *Third ERTS Symposium*, NASA SP-351, vol. 1, NASA, Washington DC, pp.309-317.

Running, S. W., C. O. Justice, V. Solomonson, D. Hall, J. Baker, Y. J. Kaufmann, A. H. Strahler, A. R. Heute, J. P. Muller, V. Vanderbilt, Z. M. Wan, P. Teillet, and D. Carneggie, 1994. Terrestrial

Remote Sensing Science and Algorithms Planned for EOS/MODIS, *Int. Journal of Remote Sensing*, 15(17): 3587-3620.

Scherrer, H. U.,1993. Projekt zur flachenhaften Erfassung und Auswertung von Sturmschaden, *AFZ/Der Wald*, 14: 712-714.

Schmidtke, H., 1993. Die fraktale Geometrie von Sturmschaden-flächen im Wald, *AFZ/Der Wald*, 14: 710-712.

Mason, S., H. Ruther, and J. Smit, 1997. Investigation of the Kodak DCS460 digital camera for small-area mapping, *ISPRS Journal of Photogrammetry & Remote Sensing*, 52(5): 202-214.

Toth, C. and D. A. Grejner-Brzezinska, 1998. Performance analysis Ž. of the airborne integrated mapping system AIMSe, *Int. Ž. Arch. Photogr. Remote Sens.*, 32(2): 320-326.

G. J. C. Underwood, and J. Kromkamp, 1999. Primary production by phytoplankton and microphytobenthos in estuaries. *Advances in Ecological Research*, 29: 93-153.